38

National Aeronautics and Space Administration
Washington 25, D. C.

Covering the period 20 April thru 19 July 1964

GEOPHYSICS CORPORATION OF AMERICA
Bedford, Massachusetts

PLANETARY METEOROLOGY

Quarterly Progress Report No. 1

Contract No. NASw-975

TABLE OF CONTENTS

SECTION 1

INTRODUCTION

The general objective of the contract is to improve our knowledge of the meteorology of the planets Mars, Venus, and Jupiter. Primary emphasis is placed on the thermal state and circulation regimes in these planetary atmospheres.

During the past three months emphasis has been on: 1) development of a model for computing the radiative equilibrium temperature in a planetary atmosphere with a complete cloud cover (such as the Venus atmosphere); 2) studies of models for estimating average wind velocities and the general circulation characteristics of the atmospheres of Mars and Venus; and, 3) uncertainties associated with the recent estimate of Martian surface pressure. These topics are discussed in the following sections.

SECTION 2

METEOROLOGY OF VENUS

2.1 RADIATIVE EQUILIBRIUM TEMPERATURE DISTRIBUTION IN THE VENUS ATMOSPHERE

In Quarterly Progress Report No. 4 of Contract No. NASw-704 the radiative equilibrium distribution of temperature between the cloud-base and surface of Venus is discussed. This computation of radiative equilibrium temperature was based upon a model in which it is assumed that the cloud layer completely covers the sky; both the cloud-base and surface radiate as black bodies; the atmospheric layer between surface and cloud is a grey absorber and is in infrared radiative equilibrium; and both the cloud base and surface are maintained at fixed temperatures, which are chosen to be in agreement with present indications of these quantities. The surface temperature was taken as $700^{\circ}K$; the cloud-base temperature was taken as $373^{\circ}K$. Temperature profiles were computed for several values of atmospheric infrared opacity. When compared to an adiabatic profile, the computed temperature profiles all indicate super-adiabatic lapse-rates at the surface-atmosphere and cloud-atmosphere boundaries.

It is of interest to develop a model that can be used to compute the radiative equilibrium temperature distribution not only of the sub-cloud layer or above-cloud layer but also of the entire atmosphere of a planet, such as Venus, that has a complete cloud cover. We have started work in this direction.

It is assumed that the Venus atmosphere is grey in the infrared and has a complete cloud cover at some height in the atmosphere. The cloud is assumed to behave as a black body for infrared radiation. The infrared opacity is taken as zero at the surface of the planet and increases to the value τ_g at the top of the atmosphere. In the sketch below, the physical model is shown schematically.

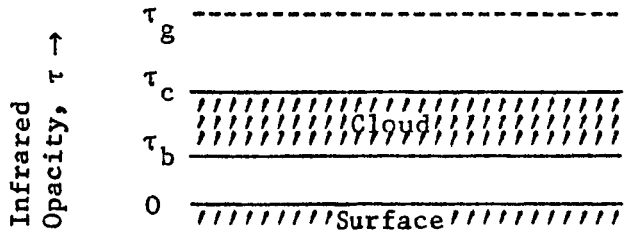

Under conditions of radiative equilibrium, the radiation fluxes at the surface, the cloud-base, the cloud-top, and top of the atmosphere are all equivalent; in particular, they are all equal to the incoming solar radiation. This can be written as

$$F(\tau_g) = F(\tau_c) = F(\tau_b) = F(o) = B_e = \sigma T_e^4 \qquad (1)$$

where T_e is the effective temperature of the incoming solar radiation, τ is the infrared opacity, and σ is the Stefan-Boltzmann constant.

The radiative flux at any level above the cloud can be written as

$$F(\tau) = 2B_c E_3(\tau-\tau_c) + 2\int_{\tau_c}^{\tau} B(t)\, E_2(\tau-t)dt - 2\int_{\tau}^{\tau_g} B(t)\, E_2(t-\tau)dt \qquad (2)$$

where B is the black body flux, the sub-script c refers to the cloud-top, and the E's are exponential integrals.

For radiative equilibrium, $\frac{dF}{d\tau} = 0$. Applying this condition to Equation (2), we can obtain

$$2B(\tau) = B_c E_2(\tau-\tau_c) + \int_{\tau_c}^{\tau_g} B(t)\, E_1\,(|\tau-t|)\, dt. \qquad (3)$$

From the condition that the upward flux at the top of the atmosphere is equal to the incoming solar radiation, we obtain

$$2B_c E_3(\tau_g-\tau_c) + 2\int_{\tau_c}^{\tau_g} B(t)\, E_2(\tau_g-t)dt = B_e \quad . \qquad (4)$$

Substituting B_c from Equation (4) into Equation (3) and replacing B by σT^4, we obtain an equation for the temperature distribution above the cloud-top

$$T^4(\tau) = \frac{T_e{}^4 E_2(\tau-\tau_c)}{4E_3(\tau_g-\tau_c)} - \frac{\left[\int_{\tau_c}^{\tau_g} T(t)^4 E_2(\tau_g-t)dt\right] E_2(\tau-\tau_c)}{2E_3(\tau_g-\tau_c)} + \frac{\int_{\tau_c}^{\tau_g} T(t)\, E_1\,(|\tau-t|)\, dt}{2} \quad . \qquad (5)$$

Given T_e, τ_c, and τ_g, one can compute $T(\tau)$ above the cloud-top from Equation (5) using numerical methods. The temperature at the cloud-

top can then be obtained from Equation (4) if B is replaced by σT^4.

Below the cloud-top, application of the radiative equilibrium condition $\frac{dF}{d\tau} = 0$ to the expression for the radiative flux results in

$$2B(\tau) = B_o E_2(\tau) + B_b E_2(\tau_b - \tau) + \int_o^{\tau_b} B(t) E_1(|\tau - t|)dt \quad . \quad (6)$$

From the condition that the infrared radiative flux at the surface is equal to the incoming solar radiation, we obtain

$$B_o - 2B_b E_3(\tau_b) - 2 \int_o^{\tau_b} B(t) E_2(t)dt = B_e \quad . \quad (7)$$

Substituting B_b from Equation (7) into Equation (6) and replacing B by σT^4, we obtain

$$T^4(\tau) = \frac{1}{2} \left\{ T_o^4 E_2(\tau) + \frac{E_2(\tau_b - \tau)}{2E_3(\tau_b)} \left[T_o^4 - T_e^4 - 2 \int_o^{\tau_b} T^4(t) E_2(t)dt \right] \right.$$

$$\left. + \int_o^{\tau_b} T^4(t) E_1(|\tau - t|)dt \right\} \quad . \quad (8)$$

Given T_e, T_o, τ_b, and τ_g, one can compute $T(\tau)$ below the cloud-base from Equation (8) using numerical methods. The temperature at the cloud-base can then be obtained from Equation (7) if B is replaced by σT^4.

Thus, given the incoming solar radiation; the surface temperature (or, if the derivation is changed slightly, the cloud-base temperature); the infrared opacity of the above cloud layer; and the infrared opacity of the sub-cloud layer, it is possible to determine the radiative

equilibrium distribution of temperature in the atmosphere both above and below the cloud.

We have computed the temperature distribution for the following values of the parameters:

$T_e = 237^{\circ}K$ $\quad \tau_g = 7.0$ $\quad \tau_b = 6.86$

$T_o = 700^{\circ}K$ $\quad \tau_c = 6.995$

$T_e = 237^{\circ}K$ corresponds to an albedo of 0.73 as reported by Sinton (1962). $T_o = 700^{\circ}K$ is in agreement with the radiometric observations of surface temperature. $\tau_g = 7$ agrees with the value of τ_g that resulted in a surface temperature of $700^{\circ}K$ for the two-layer greenhouse model (Ohring et al, 1964) with atmospheric lapse-rate and cloud-top pressure after Kaplan (1962). Since τ is proportional to atmospheric pressure for this model, τ_c and τ_g were chosen so that the ratios τ_c/τ_g and τ_b/τ_g were the same as the ratios p_c/p_o and p_b/p_o, respectively, where p_o is surface pressure. The ratio p_c/p_o, after Kaplan (1962), is about 7×10^{-4}. If the cloud-base temperature is about $373^{\circ}K$ (Staff, Jet Propulsion Laboratory), Kaplan's temperature-pressure relationships yields $p_b/p_o = 2 \times 10^{-2}$. Therefore, $\tau_c = 6.995$ and $\tau_b = 6.86$.

The computed temperature distribution is shown in Figure 2.1. It should be noted that the above-cloud temperatures and opacities are plotted on scales different from the sub-cloud scales. The temperature remains essentially constant in the sub-cloud layer, decreasing from

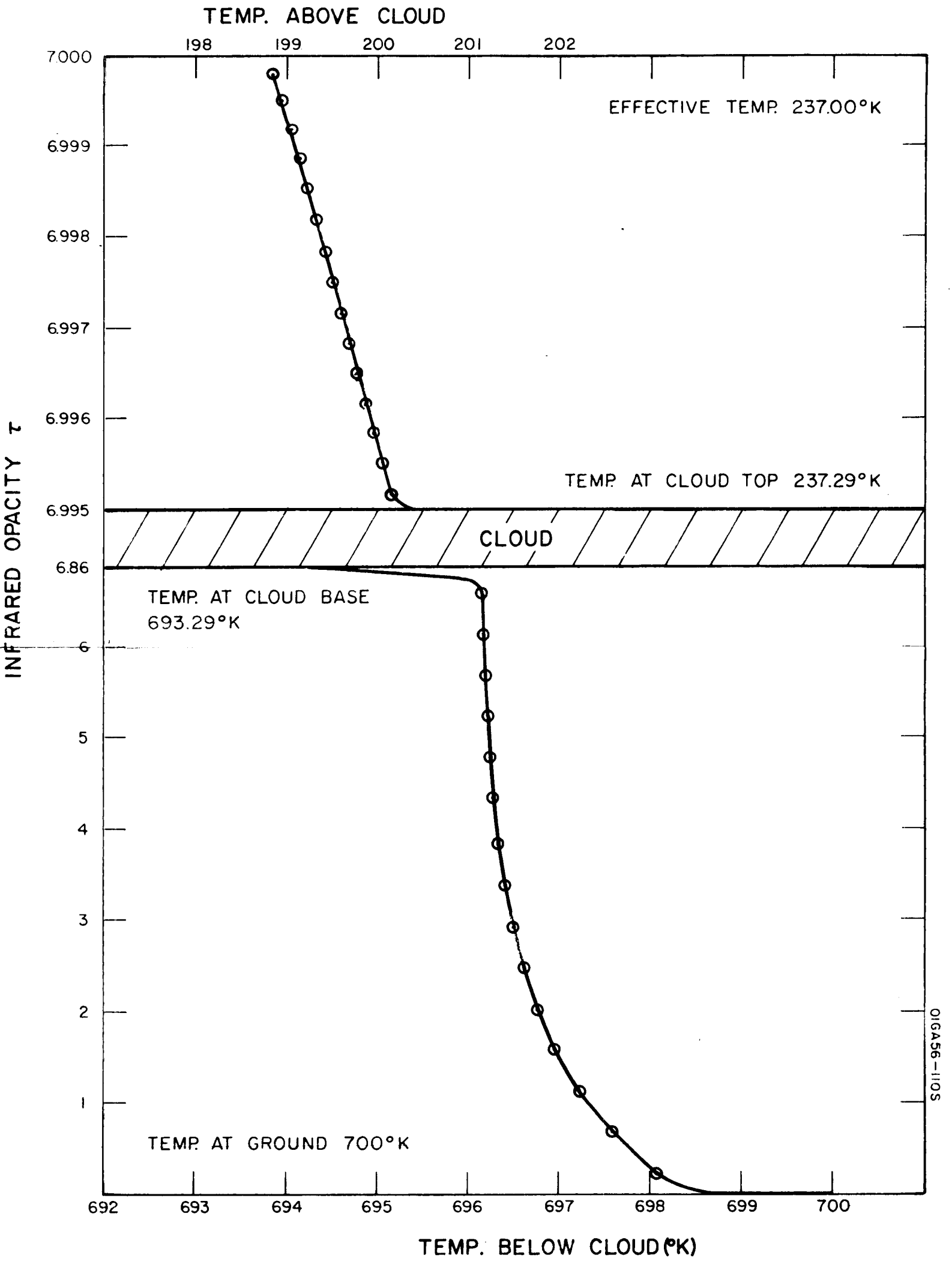

Figure 2.1 Computed radiative equilibrium temperature distribution in the Venus atmosphere. (Note different scales for above and below cloud distribution.)

700°K at the surface to 693°K at the cloud-base. In the above-cloud layer, the temperature is also essentially constant, 200°K to 199°K, except for the discontinuity at the cloud-base, where the temperature changes from slightly more than 237°K at the cloud-top to less than 200°K immediately above the cloud-top. Thus, the computed temperature distribution indicates that the atmosphere consists of essentially two isothermal layers - a sub-cloud layer with a temperature close to 700°K and an above-cloud layer with a temperature of about 200°K. There is a large temperature decrease - over 450°K - from cloud-base to cloud-top. Such a temperature distribution is quite unrealistic.

The unreasonable temperature distribution obtained below the cloud and the large temperature decrease through the cloud are probably due to the relatively small value of effective temperature compared to the surface temperature and to the assumption of a completely black cloud. Work is underway on the development of a model in which the cloud is not completely black to infrared radiation. Such a model should allow more realistic temperature distributions to be obtained.

2.2 CIRCULATION STUDIES

2.2.1 Mean Wind Velocity. Based on recent evidence, the rotation rate of Venus is about 250 days (Barath, 1964), and, therefore, the Coriolis parameter is about 4×10^{-3} times of that on Earth. With such a small rotation rate, it is highly probable that the general circulation is mainly along the meridional direction (here we define the meridional direction in the direction of the lines joining the subsolar and antisolar points, while the zonal direction is in the direction normal to the lines joining subsolar and antisolar points) and that zonal motion is small.

With a solar constant of 4.11 cal/cm^2/min and an albedo of 0.75, the effective insolation for Venus is about 1.03 cal/cm^2/min. Assuming that the surface pressure is 10 atmospheres, and the outgoing radiation is constant all over the planet, we obtain the differential heating between the subsolar and antisolar points, as

$$\alpha = 7.5 \times 10^{-6} \text{ deg/sec.}$$

Based on the model temperature profile of Kaplan (1962), and a coefficient of friction ($K = 5 \times 10^{-5}$ sec $^{-1}$) five times of that on Earth the steady state meridional velocity is

$$V_a = 3.12 \text{ m/sec.}$$

For the same friction coefficient as that on Earth ($K = 10^{-5}$/sec),

$$V_a = 18.3 \text{ m/sec.}$$

2.2.2 Linearized Circulation Model. Since there is some information available on the temperature variation between subsolar and antisolar points, we can estimate the average wind velocities using a different approach. This approach is based upon a free convection model, and has been used successfully for model circulation systems in which rotation effects are unimportant, such as the circulation patterns associated with land and sea, or valley and mountain, circulations. Using the Boussinesq approximation (Chandrasekhar, 1961), one may obtain the following equations from the equation of motion and heat equation:

$$\nu \Delta^2 u = g\alpha \frac{\partial^2 T}{\partial x \, \partial z}$$

$$\nu \Delta^2 w = -g\alpha \frac{\partial^2 T}{\partial x^2}$$

and

$$\kappa \Delta T = -\gamma_o \left[\left(\frac{\Gamma_d}{\gamma_o} + (1+bx) \right) w + bzu \right]$$

where ν, κ = eddy viscosity and eddy conductivity

α = coefficient of volume expansion for atmosphere

γ_o, Γ_d = mean lapse rate and dry adiabatic lapse rate

b = constant determining the change of lapse rate in meridional direction

Δ = Laplacian operator

When the lapse rate is independent of horizontal location, one obtains

$$\Delta^3 T = -\frac{g\alpha\gamma}{\nu\kappa} \frac{\partial^2 T}{\partial x^2}$$

where $\gamma = \Gamma_d - \gamma_o$.

The surface temperature distribution on Venus (Drake, 1964) is

$$T = \left[621 + 73 \cos(\varphi + 11.7)\right]\ ^{o}K$$

where φ is the phase angle. The above expression can be thought of as representing the temperature variation from subsolar to antisolar point on the planet with φ representing the angle between subsolar point and any point on the surface along the meridional direction. If we neglect the phase shift angle of 11.7^{o}, the perturbation temperature is just a simple single cosine function with an amplitude $73^{o}K$. Using this as the lower boundary condition one can solve the last differential equation as a boundary value problem. Further, we may assume u and w are both zero at surface as additional boundary conditions for determining the velocities. The solutions are assumed finite at $z \to \infty$.

The solutions for u, w, and T are obtained as follows:

$$u = \frac{\kappa\lambda^3 k^2 D}{2\gamma}\left\{e^{-\lambda kz} - \left[\cos\sqrt{\frac{3}{2}}\,\lambda kz + \sqrt{\frac{3}{3}}\sin\sqrt{\frac{3}{2}}\,\lambda kz\right] e^{\frac{-\lambda kz}{2}}\right\} \cdot$$

$$\cdot \sin kx \sin\varphi$$

$$w = \frac{\kappa D(\lambda k)^2}{2\gamma}\left\{e^{-xkz} - \left[\cos\sqrt{\frac{3}{2}}\,\lambda kz - \sqrt{\frac{3}{3}}\sin\sqrt{\frac{3}{2}}\,\lambda kz\right] e^{\frac{-\lambda kz}{2}}\right\} \cdot$$

$$\cdot \cos kx \cos\varphi$$

and

$$T = \frac{D}{2}\left\{e^{-\lambda kz} + \cos\left(\sqrt{\frac{3}{2}}\,\lambda kz\right) e^{\frac{-\lambda kz}{2}}\right\} \cos kx \cos\varphi$$

where D = amplitude of temperature disturbance

$\kappa = \nu$ = eddy conductivity or viscosity

$k = \frac{1}{r_o}$

r_o = radius of Venus

$\lambda = 2\left[\frac{g\alpha\gamma}{\nu\kappa}\Big/k^4\right]^{1/6}$

for $\kappa = \nu = 10^3$ m^2/sec

$g = 8.8$ m/sec^2

$D = 73^\circ$K

$r_o = 6100$ km

$k = 1.64 \times 10^{-4}$/km

$\alpha = 0.02$

$\gamma = 2^\circ$/km

$\lambda = 605$

The computed horizontal and vertical wind velocities, and perturbation temperature are plotted as a function of height in figure 2.2.

From figure 2.2 it is seen that the maximum horizontal wind velocity is about 35 m/sec (78 mph) and is located approximately at 8 km above the solid surface in the direction toward subsolar point. The maximum return flow is about 20 m/sec at 35 km above surface in the direction toward antisolar point. The computed maximum vertical velocity is about 2.0 cm/sec and is located at 28 km; the vertical velocity decreases to zero at 50 km above the surface. The perturbation temperature decreases upwards from the surface to a minimum at 30 km and then remains approximately constant.

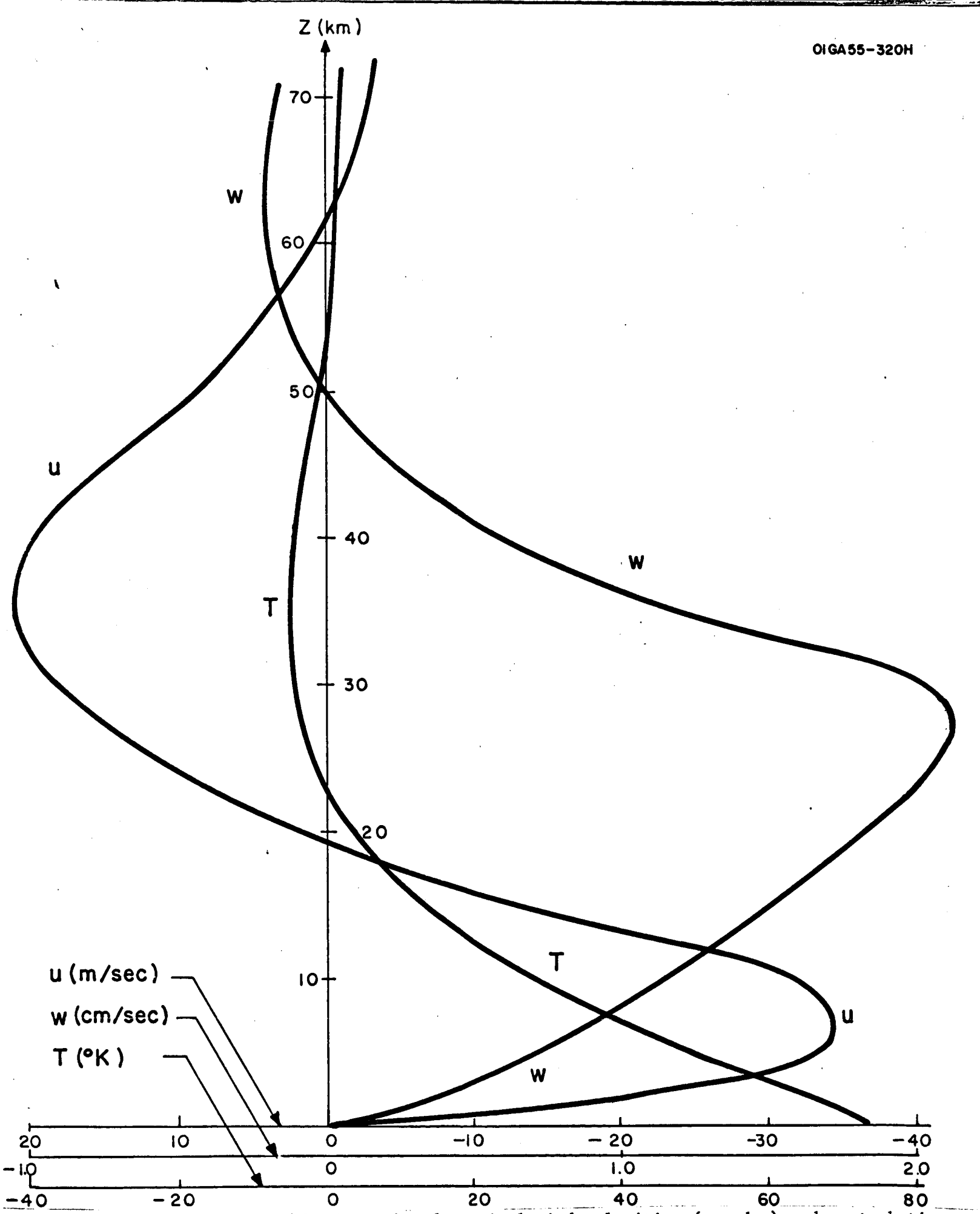

Figure 2.2 Computed horizontal and vertical wind velocities (u and w) and perturbation temperature (T) for Venus atmosphere ($\kappa=\nu=10^3 m^2/sec$; $g=8.8 m/sec^2$; $D=73^oK$; $r=6100km$; $k=1.64^{-4}/km$; $\alpha=0.002$; $\gamma=2^o/km$; $\lambda=605$; $\varphi=\pi/2$ for u, and $\varphi=0$ for w and T).

The computations show that upward vertical velocities extend to 50km on the sun-lit side of the planet, and downward vertical velocities extend 50km on the dark side of the planet. Since upward vertical velocities may extend to 50km, clouds may extend to this same altitude. However, on the dark side of the planet, above the antisolar point, where descent is taking place, the presence of clouds is a mystery.

2.2.3 Diverging Cloud Bands. A radial spoke system of clouds has been observed on Venus (Moore, 1957). This pattern has not been satisfactorily explained. According to the study of vortex clouds in hurricanes (Tang et al., 1964) and other related works (Kuo, 1963), clouds in a thermally unstable, stratified medium will orient themselves along the wind direction. If, as is probable, the Venus atmosphere may at times be unstably stratified, then the cloud bands would be oriented along the mean wind direction which is toward the subsolar point in the lower part of the atmosphere and is diverging away from the subsolar point in the upper part of the atmosphere. The resulting pattern would be in agreement with the radial spoke systems observed in Venus.

2.2.4 Future Work. More refined estimates of the Venus circulation will be obtained. In particular, the case in which the lapse rate varies with horizontal distance will be studied. Also, attempts will be made to solve a non-linear model of the Venus circulation.

SECTION 3

METEOROLOGY OF MARS

3.1 MARTIAN SURFACE PRESSURE, CARBON DIOXIDE AND WATER VAPOR AMOUNTS

In an interesting article, Kaplan, Münch, and Spinrad (1964) made an analysis of the Martian atmosphere from a high-dispersion spectrogram obtained at Mount Wilson Observatory last year, with the aid of earlier work by Sinton and Kuiper. In computing the effective air mass of sunlight reaching the surface of Mars and scattering to the Earth, they neglected the difference between the Martian latitudes, D_S and D_E, of the subpoints of the Sun and Earth, respectively. See Figure 3.1. From the 1963 American Ephemeris and Nautical Almanac, page 322, $D_S = 23^\circ16'$ and $D_E = 14^\circ44'$ for 05:10 U.T., April 13, 1963, the middle of the exposure of the photographic emulsion. The difference $D_S - D_E = 8^\circ32'$, which is much greater than the 2° value stated in the article. If D_S is increased $8^\circ32'$ from the assumed value of $D_S = D_E$ ($14^\circ44'$), the average effective path length, η, must be increased by 0.6. It turns out that the atmospheric parameters are sensitive to η and consequently need revision.

Two other refinements were made. One was to allow for the curvature of Mars' surface and atmosphere, and the other was to double the smearing

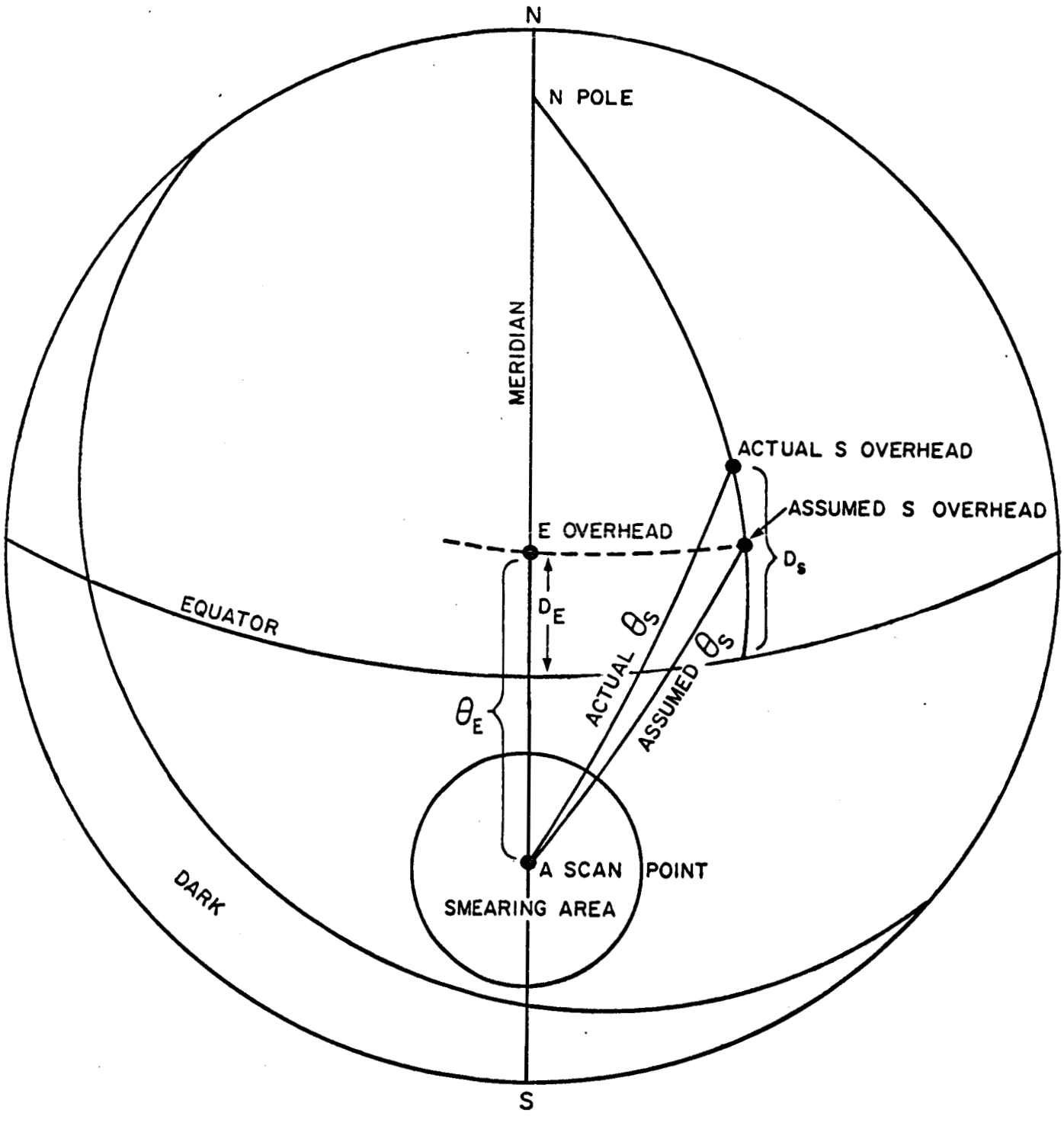

E = EARTH

S = SUN

D = PLANETOCENTRIC (MARTIAN) LATITUDE

θ = ZENITH DISTANCE AS SEEN FROM CENTER OF SCAN ON MARS

Figure 3.1 View of Mars from the Earth.

from 1 to 2 arc secant to allow for the greater scintillation associated with the turbulent north wind blowing over the mountain. In the first refinement, sec θ was replaced by

$$\sqrt{\left(\frac{R}{z}\right)^2 \cos^2\theta + \frac{2R}{z} + 1} - \frac{R}{z}\cos\theta$$

for both the Sun and Earth (θ = zenith angle at a scan point on Mars, R = radius of Mars, and z = thickness of Martian atmosphere, assumed to be 55 km). The curvature correction to η was - 0.1. The smearing effect was computed by using the center of the smearing circle (Figure 3.1) as representative of the whole circle and by keeping this circle within the scanned area along the Martian meridian. The smearing correction to η was - 0.2.

The total of the three corrections to η was + 0.6 - 0.1 - 0.2 = + 0.3, giving a revised value of η = 3.6 + 0.3 = 3.9, an increase by a factor of 13/12 (See Table 3.1). With this new value of η, the revised concentrations of carbon dioxide and water vapor are reduced by the factor of 12/13, since η w = constant. The Martian surface pressure is increased from 25 mb to 28 mb, but this is well within the $\pm$ 15 mb uncertainty expressed by Kaplan et al.

It is apparent that new observations are needed to get more reliable evaluations of the Martian atmospheric parameters.

TABLE 3.1

CARBON DIOXIDE, WATER VAPOR, AND TOTAL PRESSURE
OF MARTIAN ATMOSPHERE

Martian Atmospheric Parameter	Stated Value	Revised Value
Effective air mass, η	3.6	3.9
$w(CO_2)$ at $230^{\circ}K$	55 m atm	51 m atm
$w(CO_2)$ at $200^{\circ}K$	50 m atm	46 m atm
$w(H_2O)$	14μ	13μ
p from Sinton's measurements	29 mb	31 mb
First p from Kuiper's measurements	33 mb	36 mb
Second p from Kuiper's measurements	25 mb	27 mb
Average p from Kuiper's measurements	29 mb	31½ mb
Adjusted average p from Kuiper's measurements	25 mb	28 mb

w = total thickness at standard temperature and pressure

p = atmospheric pressure at the Martian surface

3.2 CIRCULATION STUDIES

3.2.1 Inferences from Clouds. Most yellow or white clouds have velocities over 10 km/hr. Some recorded migrating velocities, especially for yellow clouds, have reached 90 km/hr. One series of yellow clouds was generated in the same region and in the same season. The clouds followed similar paths over distances of thousands of miles from lower latitudes to higher latitudes over time periods of two weeks. Since these cloud tracks were found in southern hemisphere summer, it is suspected that they represent phenomena similar to the tropical cyclones on the Earth moving along the periphery of a subtropical permanent "high" center. The region of Moeris-Libya (+ 10°, 270°) would correspond to the Caribbean Sea or Caroline Islands in the equatorial area of Earth.

Other useful meteorological information can be deduced from observations of the vertical development of Martian clouds. In Figure 3.2 are shown examples of clouds observed on the morning terminator (after DeVaucouleurs, 1954). It was reported that the dull grey cloud, sloping upward from the surface, extended more than 40 degrees in longitude and remained visible for three hours with a top at about 27 km. In the second case, although the high cloud separated from the surface, it still remained tilted like a frontal cloud, and extended to a height of at least 30 km. These observations show that these clouds extend to very high altitudes and have sloping surfaces just like a schematic terrestrial front.

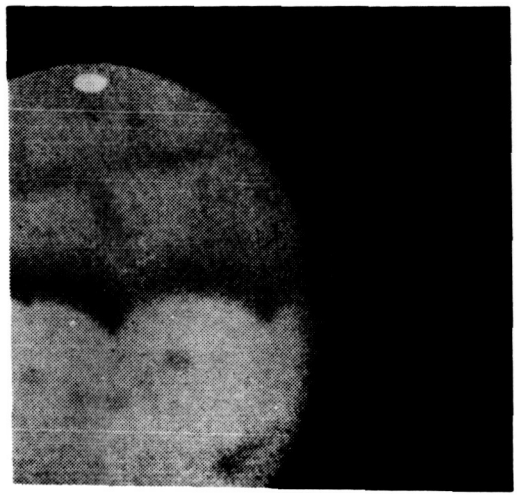

1.

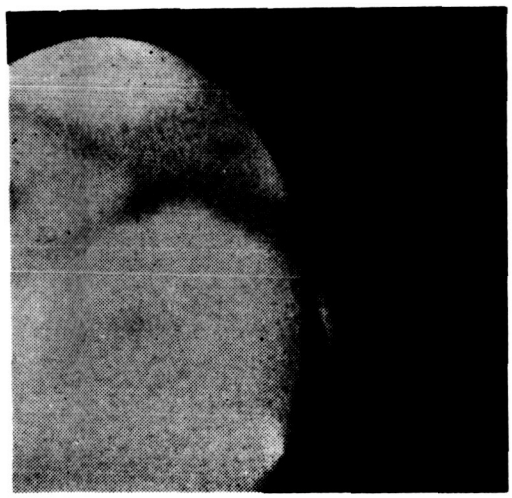

2.

Figure 3.2 Observations of clouds on the terminator.
Case 1. The dull-grey cloud extended over more than 40 degrees in longitude and remained visible for 3 hours with a top at about 27 km.
Case 2. The dark-yellow cloud, which appeared separated from the surface, remained tilted like a frontal cloud, and extended to a height of at least 30 km.
(After DeVaucouleurs, 1957)

Implications of these phenomena for the fluid dynamics of the atmosphere will be discussed in the next few sections.

3.2.2 The Slope of a Front. The cloud pictures shown in Figure 3.2 resemble a terrestrial front, which is characterized by its coverage of a large area and by the sloping, relatively narrow cloud band above its surface. Furthermore, the fact that these cloud phenomena are observed on the terminator suggests that they are not convective clouds for the following reasons. Convection must be weakest at the time of sunrise on a desert-like planet. Also, the sloping narrow cloud band bears no resemblance to a convective cloud with strong vertical development on the Earth.

The slope of a terrestrial front at middle latitudes is about 1/50 to 1/100; the slope of these Martian clouds are much larger. The expression for the slope of an east-west front at low latitudes can be written as

$$\tan \alpha = - \frac{\rho_1 \left(U \frac{\partial U}{\partial x} - fV \right)_1 - \rho_2 \left(U \frac{\partial U}{\partial x} - fV \right)_2}{-(\rho_1 V_1 - \rho_2 V_2) \frac{\partial f}{\partial \varphi} + g(\rho_1 - \rho_2)}$$

where α = the angle between the frontal surface and the horizontal surface

ρ = density of air

f = Coriolis parameter

φ = latitude

g = gravitational constant

x,y = the coordinate system in which x and y are in the direction normal and parallel to the surface front in the horizontal surface respectively.

U,V = velocities along x- and y-direction respectively

and, the subscripts 1 and 2 denote the cold and warm air masses respectively.

At lower latitudes one would not expect too large a temperature contrast and, therefore, one can assume that

$$\tan \alpha \approx - \frac{f(V_1 - V_2) + \left(U \frac{\partial U}{\partial x}\right)_1 - \left(U \frac{\partial U}{\partial x}\right)_2}{\frac{\partial f}{\partial \varphi}(V_2 - V_1)} \quad .$$

Furthermore we may assume that the mean warm air velocity is negligibly small (i.e., $U_2 = 0$) and that the mean velocity gradient in the cold air is constant. $\left(\frac{\partial U_1}{\partial x} = \text{constant} = -c\right)$. With these approximations, the slope of the front can be written as

$$\tan \alpha = \tan \varphi + \frac{|c\ U_1|}{2\omega \cos\varphi |V_1 - V_2|} \quad .$$

The value c may be estimated as

$$c = \frac{10 \text{ m/sec}}{20 \times 10^5 \text{ m}} = \frac{1}{2} \times 10^{-5}/\text{sec}.$$

Further assume

$$|U_1| = 40 \text{ m/sec}$$

$$|V_1 - V_2| = 10 \text{ m/sec}$$

$$2\omega = 1.5 \times 10^{-4}/\text{sec}$$

$$\varphi = 5^{\circ} \text{ latitude}$$

then

$$\tan \alpha \approx 0.22$$

and

$$\alpha \approx +12^{\circ} \quad .$$

This value agrees well with the slope of the clouds shown in Figure 3.2. If these clouds are indeed representative of frontal phenomena on Mars, in agreement with the above computation, then they are most probably composed of ice rather than dust.

3.2.3 The Circulation Regime. For large scale motions, the Earth's atmosphere is in a state of quasi-geostrophic or geostrophic balance, which means that the horizontal motion is established mainly under the primary balance between the Coriolis force and the pressure gradient force. It is interesting to find out whether the large scale Martian atmospheric motions are in a similar state of quasi-geostrophic balance. The criterion of geostrophic balance is based on a non-dimensional number which is directly proportional to the thermal wind, namely, the thermal Rossby number, R^{*}_{oT}. If the thermal Rossby number is between 0.1 and 0.01, the atmospheric motion is approximately in geostrophic balance (Davis, 1958).

For the appropriate Martian physical parameters and for the mean daily temperature difference between pole and equator as given by Ohring, Tang and DeSanto (1962), we have

$$R^*_{oT} = 0.053$$

in the mean for the year. This is compatible with the value of the thermal Rossby number for the terrestrial atmosphere from Mintz's (1955) data for 1949 (See Fultz et al., 1959)

Season	R^*_{oT}
Summer	0.027
Winter	0.054

Since R^*_{oT} in the Martian atmosphere is of the same order of magnitude as in the Earth's atmosphere, the mean annual atmospheric motions on Mars are in geostrophic or quasi-geostrophic equilibrium, as on the Earth.

Furthermore, with the thermal Rossby number, R^*_{oT}, and the rotation parameter, G^*, which is inversely proportional to the square of the angular velocity, one can determine whether the circulation regime is a symmetric or wave type; and, if it is a wave type, one can determine the preferred wave number of the circulation. Based on the physical parameters of the planet we can determine G^*. From the computed values of R^*_{oT} and G^*, we obtain the result that the Martian atmosphere is in a wave regime with a preferred wave number of about five, which is similar to the wave number for the terrestrial general circulation.

On the other hand, Mintz (1961) reached a different conclusion. Using a two-level model and assuming the motion is geostrophic, he derived a criterion for the stability of a circulation regime. The criterion is directly proportional to the dynamic coefficient of eddy viscosity at 500 mb. If the actual total poleward heat transport, ΔQ, is less than the critical value, ΔQ_{crit}, a symmetrical circulation will be dynamically stable. Based on his assumed data, Mintz obtained

$$\Delta Q_{crit} = 0.17 \times 10^{12} \text{ kj/sec}$$

and

$$\Delta Q = 0.12 \times 10^{12} \text{ kj/sec}$$

for yearly Martian means, and concluded that the general circulation of Mars is symmetrical and dynamically stable. However, it is worthwhile to note that the coefficient of eddy viscosity he used may be twice as large as in the mean atmosphere. Mintz adopted μ = 220 gm/cm/sec from Palmén (1955a), who used this value for lower latitude on Earth. However, later Palmén (1959) assumed μ = 100 gm/sec/cm in the computation for the mean frictional dissipation in the layer 1-12 km in the terrestrial atmosphere. Other workers, Schmidt (1925), Rossby and Montgomery (1935), Brunt (1939), Haurwitz (1941), and recently Palmén (1959), have assumed that μ is approximately 100 gm/sec/cm in the free atmosphere or even in the planetary boundary layer of the Earth. If this lower value of μ is used in Mintz's criterion, then the conclusion is reached that the general circulation on Mars is in a wave regime in the mean for the year. This is in agreement with the conclusion based upon the thermal Rossby number in the rotation parameter approach.

3.2.4 Mean Zonal and Meridional Wind Velocity of General Circulation.

The annual radiation budget for Mars as computed by Ohring et al. (1964) gives the total difference of heating per unit area between the equator and pole:

$$\Delta[S(1 - A) - W] = 0.04 \text{ cal/cm}^2\text{/min}$$

where Δ = difference of the quantities in the brackets between the equator and the pole

S = solar constant for Mars

A = albedo

W = outgoing long-wave radiation.

For a surface pressure $p_1 = 25$ mb, the difference in the rate of temperature change between equator and pole is

$$\frac{dT}{dt} = 4.2 \times 10^{-5} \text{ }^{\circ}\text{K/sec.}$$

Based on Haurwitz's (1961) general model of thermally driven large scale motion, and with a set of appropriate parameters, one can compute the steady state meridional and zonal velocities in the Martian atmosphere. One of the important parameters is the coefficient of friction. Since the atmospheric pressure on Mars is much less than on Earth, we have assumed a friction coefficient for Mars that is 1/2 the Earth's. We obtain with this model a meridional velocity of 1.5 m/sec and a zonal velocity of 30 m/sec. Results for different values of the parameters have also been obtained.

These calculations indicate that the average wind velocity on Mars is about three times as high as the average wind velocity on Earth. For individual disturbances of various scales, the wind velocities must be larger than the average values just presented. This is why some yellow clouds can be frequently observed moving with a speed of 90 km/hr. The average wind speeds on Mars are higher than on Earth because 1) the difference in radiational temperature change between equator and pole is greater on Mars than on Earth, and 2) the coefficient of friction is lower on Mars than on Earth. Both of these circumstances are indirectly due to the fact that the Martian surface pressure is lower than the Earth's.

3.2.5 Development and Profile of Large Scale Vertical Velocity and Vertical Extent of Clouds on Mars. In this section, we would like to obtain some estimates of the magnitudes and variation with altitude of the vertical velocities associated with Martian atmospheric waves. Knowledge of the height variation of the vertical velocity will enable us to estimate the maximum heights of clouds.

The simplified Omega equation (See, for example, Haltiner and Martin, 1957) for a planetary sinusoidal baroclinic wave disturbance can be written as

$$\frac{f^2}{k^2}\frac{\partial^2\omega}{\partial p^2} + \frac{S}{p}\omega = -2\frac{\partial u}{\partial p} fv + \frac{\beta f}{k^2}\frac{\partial v}{\partial p}$$

where

$k = \frac{2\pi}{L}$ = wave number

$\omega = \frac{dp}{dt}$

u, v = zonal and meridional velocities

p = pressure

$\beta = \frac{\partial f}{\partial y}$

R = gas constant for the atmosphere

$S = RT \frac{\partial \ell n\, \theta}{\partial p}$

T = temperature

f = Coriolis parameter

θ = potential temperature.

Assuming zonal and meridional velocity profiles similar to that of the Earth's atmosphere

$$u = u_o \left(1 - \frac{p}{p_o}\right)$$

$$v = v_o \left(0.4 - \frac{p}{p_o}\right),$$

where p_o = surface pressure

u_o, v_o = amplitude of the zonal and meridional velocities,

we can obtain the following complete solution for the Omega equation

$$\omega = \frac{2}{\gamma} \frac{\left[4F - \left(E + \frac{8F}{\gamma}\right)\right]}{I_1(2\,\gamma^{\frac{1}{2}})} s\, I_1(\gamma^{\frac{1}{2}} s) - \frac{F}{\gamma} s^4 + \left(\frac{E}{\gamma} + \frac{8F}{\gamma^2}\right) s^2$$

where I_1 = modified Bessel function of first kind

$F = \frac{k^2 p_o u_o v_o}{8f}$,

$\gamma = \frac{k^2 |S| p_o}{f^2}$,

$E = \frac{0.2\, k^2 p_o u_o v_o}{f} - \frac{\beta p_o v_o}{4f}$,

$s = 2\left(\frac{p}{p_o}\right)^{\frac{1}{2}}$.

For moderate and relatively short waves, the solution can be written as

$$\omega = - \frac{D}{\gamma I_1(2\gamma^{\frac{1}{2}})} \left(0.3 + \frac{1}{\gamma}\right) s\, I_1(\gamma^{\frac{1}{2}}s) + \frac{D}{16\gamma} s^4 + \frac{D}{2\gamma^2}(1 - 0.2\gamma)s^2$$

where $$D = \frac{2 k^2 p_o u_o v_o}{f} .$$

For the terrestrial atmosphere, the values of the velocity amplitudes, moderate wave length of atmospheric disturbance, and stability factor can be assumed as

$$u_o = v_o \approx 40 \text{ m/sec}$$

$$L = 4000 \text{ km}$$

$$S = 12 \text{ m}^2/\text{mb}/\text{sec}^2/\text{deg}.$$

With the above values the profile of ω, for the Earth's atmosphere is shown in Figure 3.3. The maximum vertical velocity $|w| = + \left|\frac{\omega}{\rho g}\right| = 1.7$ cm/sec, and the profile is close to the average profile in the Earth's atmosphere.

In the Earth's atmosphere, clouds do not usually extend above the tropopause. Observations indicate that the horizontal velocity divergence is a maximum at the height of the tropopause. From the equation of continuity, one can obtain the result that $\frac{\partial^2 \omega}{\partial p^2} = 0$ at a level of maximum horizontal velocity divergence. Thus, working in reverse, one can estimate the height of the tropopause, and, hence, the maximum height of frontal clouds, from an estimate of the height at which $\frac{\partial^2 \omega}{\partial p^2} = 0$. For the Earth's atmosphere,

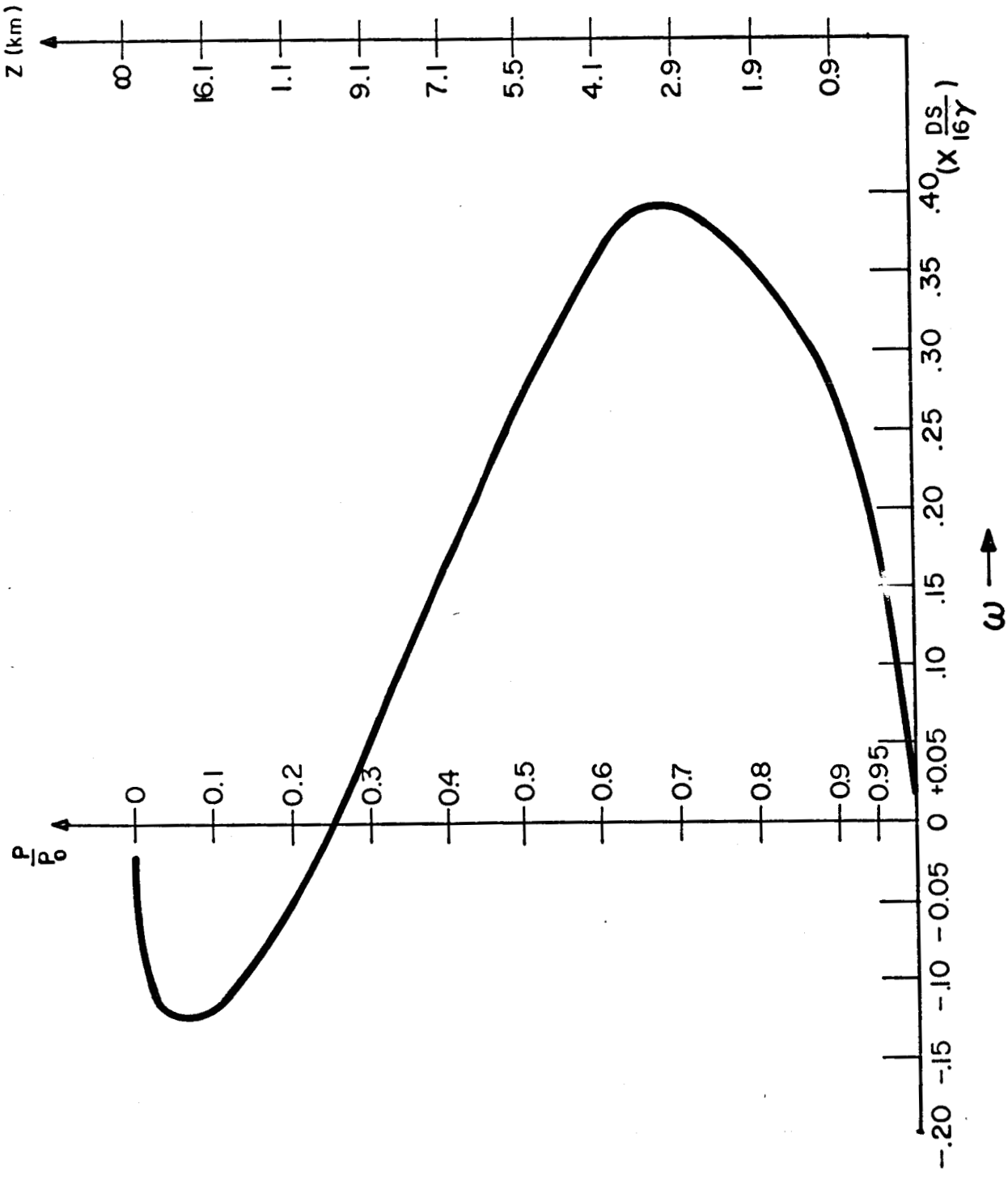

Figure 3.3 Computed vertical velocity profile for terrestrial atmosphere ($u_o = v_o$ = 40 m/sec; L = 4000 km; S = m^2/mb/sec/deg).

we obtain $\frac{\partial^2 \omega}{\partial p^2} = 0$ at about 350 mb, in reasonable agreement with the observed tropopause pressure of 250 mb at middle latitudes.

For the case of Mars, we may assume that

$$u_o = v_o = 60 \text{ m/sec}$$

$$S = 90 \text{ m}^2/\text{mb}/\text{sec}^2/\text{deg}$$

$$L = 4000 \text{ km}$$

$$\rho = 4 \times 10^{-5} \text{ gm/cm}^3.$$

The result is shown in Figure 3.4. The maximum vertical velocity is approximately

$$|w| = 12.8 \text{ cm/sec}$$

which is about one order of magnitude larger than that on Earth. Based on a 20 km scale height for the Martian atmosphere, $\frac{\partial^2 \omega}{\partial p^2} = 0$ or the tropopause would be near 20 km. Thus, observations of Martian frontal clouds at heights of 30 km (see Figure 3.2) above the surface in lower latitudes are probably correct. If frontal clouds can reach 30 km, then convective clouds on Mars can probably reach greater altitudes.

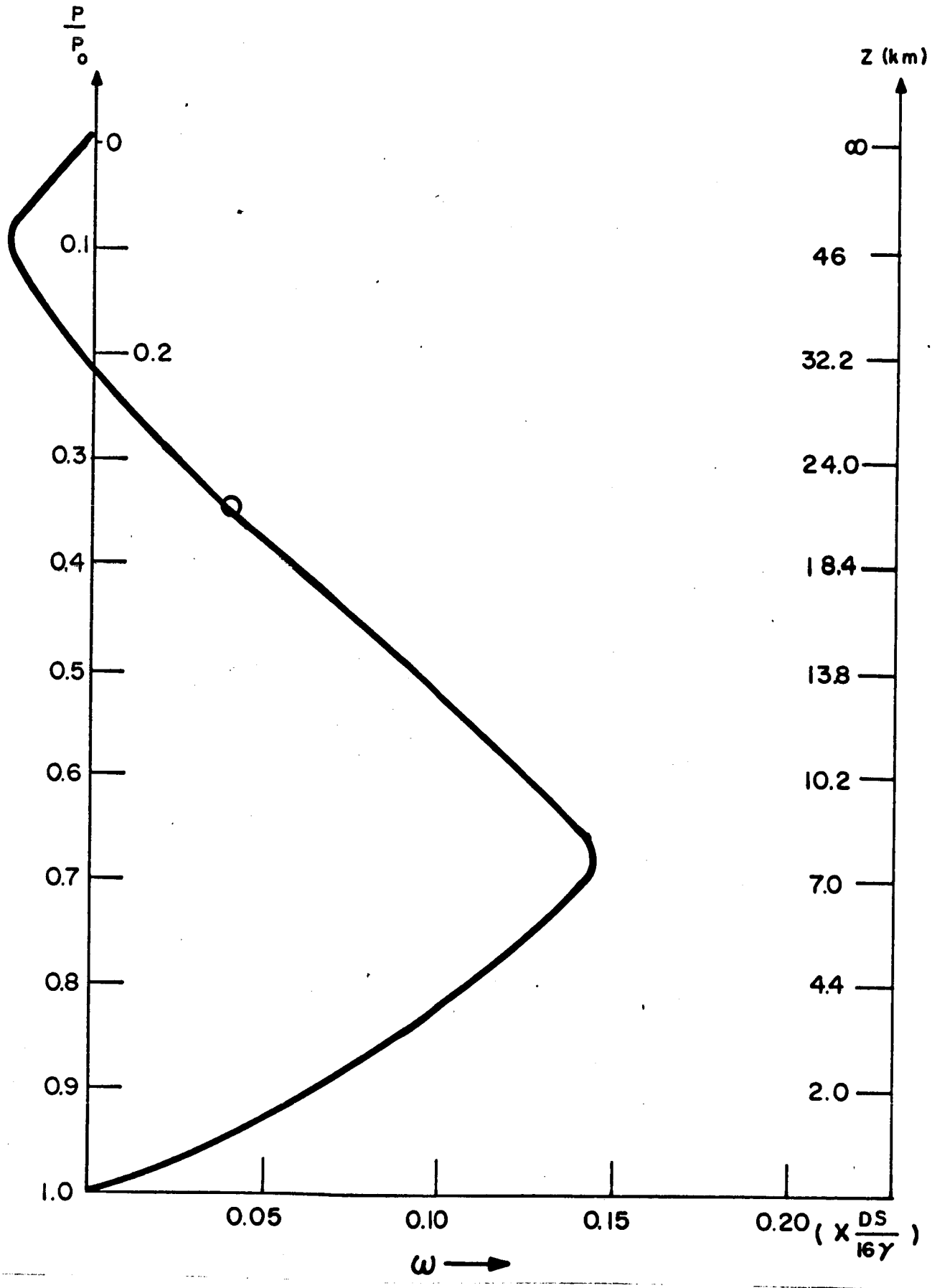

Figure 3.4 Computed vertical velocity profile for Martian atmosphere ($u_o = v_o = 60$ m/sec; L = 4000 km; S = 90 m^2/mb/sec/deg)

SECTION 4

METEOROLOGY OF JUPITER

4.1 VERTICAL VARIATION OF TEMPERATURE ABOVE CLOUDS

Work has begun on the development of a model for computing the radiative equilibrium temperature distribution above the clouds of Jupiter. It is anticipated that a non-grey radiative equilibrium model, which takes into account the variation of absorption coefficient with wavelength, will be used for these computations. Absorption of infrared radiation in Jupiter's atmosphere is primarily due to ammonia.

SECTION 5

ADMINISTRATIVE NOTES

A paper on "Changes In The Amount Of Cloudiness And The Average Surface Temperature Of The Earth" by George Ohring has been accepted for publication in The Journal of the Atmospheric Sciences and will appear in the July 1964 issue. The work reported on in the paper was supported by Contract No. NASw-704.

Dr. Ohring will present a paper on "The Greenhouse Effect in Planetary Atmospheres" at the International Symposium on Atmospheric Radiation in Leningrad, U.S.S.R., August 5-12, 1964. The work that will be reported on has been supported by our present and past NASA contracts. An abstract of this presentation follows

"The Greenhouse Effect in Planetary Atmospheres"

Average surface temperatures for the planets Mars, Venus, and Earth are calculated with the use of a simple greenhouse model for planetary atmospheres. The model permits evaluation of the influence of amount and height of clouds on the magnitude of the greenhouse effect. It is assumed that: there is a balance between incoming solar radiation and outgoing infrared radiation at the top of the

atmosphere; the atmosphere consists of two layers — a troposphere, which has a constant lapse rate, and a stratosphere, which is isothermal and in gross radiative equilibrium; the atmosphere acts as a grey absorber and clouds as black bodies in the infrared; and direct absorption of solar radiation is negligible. In addition to surface temperature, tropopause heights can be computed with the model. Computed surface temperatures and tropopause heights are compared with observational information. For the Earth, computations with different cloud amounts indicate how the average surface temperature would respond to large changes in average cloudiness.

REFERENCES

Barath, F.T., 1964: Symposium on radar and radiometric observations of Venus during the 1962 conjunction. Astronomical Journal, 69, 1-2.

Brunt, D., 1939: Physical and Dynamical Meteorology. Cambridge University Press, Cambridge, 428 pp.

Chandrasekhar, C., 1961: Hydrodynamic and Hydromagnetic Stability. Oxford, Oxford at the Clarendon Press, 653 pp.

Davis, T.V., 1959: On the forced motion due to heating of a deep rotating liquid in an annulus. Journal of Fluid Mech., 5, 593-621.

DeVaucouleurs, G., 1954: Physics of the Planet Mars. Faber and Faber, Ltd., London, 365 pp.

Drake, F.D., 1964: Microwave observations of Venus, 1962-1963. Astronomical Journal, 69, 62-64.

Fultz, D., et al., 1959: Studies of thermal convection in a rotating cylinder with some implication for large scale atmosphere motions. Meteor. Monographs, 4, AMS (1959), 104 pp.

Haltiner, G. J., and F.L. Martin, 1957: Dynamical and Physical Meteorology. McGraw-Hill Book Co., Inc., New York, 470 pp.

Haurwitz, B., 1941: Dynamic Meteorology. McGraw-Hill Book Co., Inc., New York, 365 pp.

Haurwitz, B., 1961: Thermally driven circulations in a rotating fluid system. Scientific Rpt. No. 2, Contract No. AF 19(604)-5488. 29 pp.

Kaplan, L.D., 1962: A preliminary model of the Venus atmosphere. Tech. Rpt. 32-379, Jet Propulsion Lab., C.I.T., 5 pp.

Kaplan, L.D., G. Münch, and H. Spinrad, 1964: An analysis of the spectrum of Mars. Astrophysical Journal, 139, 1-15.

Kuo, H.L., 1963: Perturbation of plane Couette flow in stratified fluid and origin of cloud streets. Physics of Fluids, 6, 195-211.

Mintz, Y., 1955: Final computation of the mean geostrophic poleward flux of angular momentum and of sensible heat in the winter and summer of 1949. Final Rpt., Contract AF 19(122)-48, U.C.L.A., 14 pp.